Effects of Polydispersity on Structuring and Rheology in Flowing Suspensions

Eilis Rosenbaum[*], Mehrdad Massoudi[†], Kaushik Dayal[‡]

[*‡]Department of Civil and Environmental Engineering, Carnegie Mellon University

[*†]National Energy Technology Laboratory, 626 Cochrans Mill Road, P.O. Box 10940, Pittsburgh, PA 15236

[‡]Center for Nonlinear Analysis, Carnegie Mellon University

[‡]Department of Materials Science and Engineering, Carnegie Mellon University

April 29, 2019

Abstract

The size and distribution of particles suspended within a fluid influence the rheology of the suspension, as well as strength and other mechanical properties if the fluid eventually solidifies. An important motivating example of current interest is foamed cements used for carbon storage and oil and gas wellbore completion. In these applications, it is desired that the suspended particles maintain dispersion during flow and do not coalesce or cluster. This paper compares the role of mono- against poly- dispersity in the particle clustering process. The propensity of hard spherical particles in a suspension to transition from a random configuration to an ordered configuration, or to form localized structures of particles, due to flow is investigated by comparing simulations of monodisperse and polydisperse suspensions using Stokesian Dynamics. The calculations examine the role of the polydispersity on particle rearrangements and structuring of particles due to flow, and the effects of the particle size distribution on the suspension viscosity. A key finding of this work is that a small level of polydispersity in the particle sizes helps to reduce localized structuring of the particles in the suspension. A suspension of monodisperse hard spheres forms structures at a particle volume fraction of approximately 47% under shear but a 47% volume fraction of polydisperse particles in suspension does not form these structures.

Keywords: Stokesian Dynamics, Fast Lubrication Dynamics, dense suspension, foamed cement, polydispersity, rheology

[*]Email: Eilis.Rosenbaum@netl.doe.gov
[†]Email: Mehrdad.Massoudi@netl.doe.gov
[‡]Email: Kaushik.Dayal@cmu.edu

1 Introduction

The motivation for this study is to better understand the viscoelastic properties of foamed well cement, due to the addition of bubbles to the cement slurry. Foamed cement is created by dispersing gas, usually an inert gas like nitrogen, into cement slurry to create a suspension composed of bubbles and solid particles. Foamed cement is used in wellbores requiring a lower density cement, such as wells drilled into weak or fractured formations [1]. In the wellbore, cement is placed between the steel casing at the center of the well and the formation. Cement is used to isolate and seal wells in carbon storage and hydrocarbon extraction and to support the casing. The process of foaming the cement slurry lowers the density of the cement as necessary for the application, without changing the cement chemistry and while maintaining its compressive strength.

Cement is a highly complex material with properties that change over time. The cement slurry is made up of the cement clinker (a powdery mix of materials - primarily lime, silica, alumina, and iron) that when mixed with water begins the chemical reaction in the form of a hydration process [2]. During the hydration process the chemical and the physical properties of the cement slurry are changing. However, during the induction period when the cement is placed in the wellbore, little hydration occurs and the slurry properties remain fairly constant. We are interested in the foamed cement properties during its placement in the wellbore.

The bubble sizes and their distribution play a key role in the properties of foamed cement, including stability [2]. The American Petroleum Institute (API) recommends foamed cement slurries be designed to have an added gas volume fraction below 35% at the placement depth for a stable foam that will maintain the mechanical integrity and the proper zonal isolation [3]. Above 35% volume fraction of gas, the permeability may increase to unacceptable levels, and the compressive strength and the ability to support the casing could be compromised. Pressures vary throughout the cement process due to different depths in the well; we, therefore, study a range of volume fractions (10% to 50%). The foam should also have well dispersed bubbles that remain suspended during placement in the well without significant clustering, coalescence, or other undesirable configuration changes until the cement fully hardens [1]. Clusters of bubbles in foamed cement could increase the permeability once cured because the bubbles can become interconnected. If the bubbles become ordered and form structures of closely configured bubbles in the set cement, they weaken the effectiveness of the cement by forming weak points for crack formation, which creates pathways for fluid to flow and compromises the strength of the cement [4, 5]. Cracks can also increase the permeability beyond the acceptable levels to provide proper zonal isolation.

Foamed cement samples produced in the laboratory that have come to a steady flow condition show bubble rearrangement due to flow and subsequent clustering of the bubbles [6]. Comparable foamed cement samples that were captured before attaining a steady flow, show no clustering of the bubbles which remained in a random configuration. It is therefore evident that the flow influences the properties of the foamed cement.

Our aim here is to study the influence of size distributions on the final arrangement of the particles under flow using numerical simulations. We use the Stokesian Dynamics method [7], in the more efficient recent Fast Lubrication Dynamics (FLD) approximation [8–10]. This method enables us to track the location of all the particles during the simulation, and thereby obtain insights into

smaller scale phenomena such as the detailed particle spatial distribution and structuring. Particles can arrange into structures, where the particles become closer together. Higher levels of structuring will show the particles arrange in a single line of particles. Structuring of any kind could result in weakness along the line of particles.

2 Approach to Mathematical Modeling of Suspensions

2.1 Background

In this section, we will provide a brief discussion of various approaches to mathematically model a complex fluid which is composed of particles suspended in a fluid. In general, we can talk about non-flowing multicomponent systems, such as composite materials (the different components can undergo elastic or plastic deformations without involving any motion), or flowing multicomponent materials such as coal or cement slurries, fluidization, etc. We will limit our discussion to a two-component flowing system, composed of particles and a host fluid. The fluid can be either a gas or a liquid and the particles can be rigid (such as sand) or deformable (such as drops or bubbles). It is possible to study (model) these flows using continuum theories, statistical theories or numerical simulations.

From a continuum mechanics perspective, there are a few ways to study a two-component (sometimes called a two-phase) system (see [11,12]). The first approach is used when the two components interact with each and each component influences the motion and the behavior of the other component. This is usually known as the Dense Phase approach, or the Eulerian (two-fluid) approach. This method can be used to study fluidization, gas-solid flows, pneumatic conveying, and suspensions, etc. These ideas can be traced back to the pioneering work of Truesdell in 1957 (see [13]) and in the context of continuum theories, they are named mixture theories (see the review articles in references [14, 15] and the book [16]). For a recent review and discussion of the relevant issues, see the two articles: [17] and [18]. The basic assumption is that at any instant of time, every point in space is occupied by one particle from each constituent. The theory provides a means for studying the motions of bodies composed of several constituents by generalizing the equations for the mechanics of a single continuum . This method is probably the most comprehensive and the most difficult method to use, since in general, it would involve solving partial differential equations and requires many constitutive relations. When thermal, chemical, and electromagnetic effects are ignored, and assuming no inter-conversion of mass between the two components, the governing equations are the conservation equations for mass, linear momentum and angular momentum for each component. These are given for the two constituents:

$$\frac{\partial \rho^i}{\partial t} + \operatorname{div}(\rho^i \boldsymbol{v}^i) = 0, \text{ where } i = s, f \tag{2.1}$$

Where s and f refer to the solid and fluid components, respectively, div is the divergence operator, $\boldsymbol{v}^i$ is the velocity vector, and ρ^i designates the density. The densities in the current and reference configuration are related through the kinematical field $\phi(x,t)$, called volume fraction (sometimes

referred to as porosity), such that:

$$\rho_s = (1-\phi)\rho_R^s \tag{2.2}$$

$$\rho_f = \phi\rho_R^f \tag{2.3}$$

Where $0 \leq \phi(\boldsymbol{x},t) \leq \phi_{max} < 1$. Thus when $\phi = 1$, there are no particles and the suspension is simply a pure fluid. Note that Equations (2.2) and (2.3) imply that the mixture is saturated. Otherwise, the porosities are constrained by $\phi_s + \phi_f \leq 1$. The balance of linear momentum for the two components is given by

$$\rho^i \frac{d^i \boldsymbol{v}^i}{dt} = \operatorname{div} \boldsymbol{\sigma}^i + \rho^i \boldsymbol{b}^i + \boldsymbol{m}^i, \text{ where } i = s, f \tag{2.4}$$

Where $\boldsymbol{b}^i$ is the external body force, $\boldsymbol{m}^i$ is the interaction forces, $\boldsymbol{\sigma}^i$ designate the partial stress tensor and $\frac{d^i(.)}{dt} = \frac{\partial(.)}{\partial t} + [\operatorname{grad}(.)]\boldsymbol{v}^i$. In the absence of couple stresses, the balance of angular momentum indicates that the total stress tensor for the mixture is symmetric. To solve these equations, at least three constitutive relations are needed: two (tensor) equations for the two stress tensors and one (vector) equation for the interaction forces, which could include terms such as drag, lift, relative acceleration (virtual mass), history effects, etc. (see [19, 20]). A point to notice is that in any of these continuum-based theories, a new kinematical field, namely the volume fraction (concentration, porosity) has been added to the list of the parameters of interests, namely, velocity, density, and pressure. For problems involving heat transfer, temperature also need to be added. Similarly, for problems dealing with chemical reactions or electro-magnetic effects additional fields will have to be introduced. Furthermore, in these mixtures-based theories, the distinct characteristics of particles, such as size, shape, surface roughness, etc., do not enter the equations in a direct manner; at best, some of the information can be included in some of the coefficients which appear in the constitutive relations such as the drag force. There are, however, micro-continuum theories, where a length scale can be introduced (see [21]).

In the second approach, the amount of the dispersed particles is so small that their motion does not affect the motion of the host fluid. This occurs in applications such as atomization, sprays, pollution, etc. This approach is known as the Dilute Phase or the Lagrangian approach. In this case, there is a one-way coupling, namely the motion of the fluid affects the motion of the particles but not the other way around. The equations which need to be solved simultaneously are the force equation for the particles (which will include a source term due to the motion of the fluid, usually in the form of interaction forces such as drag, which depends on the relative velocity) and the conservation of mass and linear momentum equations for the fluid (see [22–24]). The constitutive parameters which are needed are the stress tensor for the fluid component and the interaction forces. To obtain the basic equation governing the motion of a particle suspended or entrained in a fluid, most researchers start with the equation of motion of a single (spherical) particle in a fluid. Tchen [25] synthesized the work of Basset, Boussinesq, Stokes, and Oseen on the motion of a sphere settling under the force of gravity in a fluid at rest. The resulting equation is usually called the Basset–Boussinesq–Oseen (BBO) equation. This equation went through a series of revisions and updates; it is generally accepted that a three-dimensional form of the BBO equation in a nonuniform flow is given by Maxey and Riley (1983) [26]:

$$
\begin{aligned}
m_s \frac{\mathrm{d}\boldsymbol{v}_s}{\mathrm{d}t} =& m_f \frac{\mathrm{D}\boldsymbol{v}_f}{\mathrm{D}t} - \frac{1}{2} m_f \frac{\mathrm{d}}{\mathrm{d}t}\Big\{\boldsymbol{v}_s(t) - \boldsymbol{v}_f(t) - \frac{1}{10} a^2 \nabla^2 \boldsymbol{v}_f\Big\} \\
& - 6\pi a \mu_f \Big\{\boldsymbol{v}_s(t) - \boldsymbol{v}_f(t) - \frac{1}{6} a^2 \nabla^2 \boldsymbol{v}_f\Big\} + 6\pi a^2 \mu_f \int_0^t \mathrm{d}\tau \frac{\frac{\mathrm{d}}{\mathrm{d}t}\Big\{\boldsymbol{v}_s(\tau) - \boldsymbol{v}_f(\tau) - \frac{1}{6} a^2 \nabla^2 v_f\Big\}}{\sqrt{\pi \nu_f (t-\tau)}} \\
& + (m_s - m_f)\boldsymbol{g}
\end{aligned}
\tag{2.5}
$$

where $\boldsymbol{v}_s$ is the velocity of the particle, $\boldsymbol{v}_f$ is the velocity of the fluid, a is the particle radius, g is the acceleration of gravity, μ_f and ν_f are the dynamic viscosity and the kinematic viscosity of the fluid, respectively. The second term on the right-hand side (RHS) of Equation (2.5) reflects the presence of the virtual mass, the third term is the Stokes drag, the fourth term is the Basset history effects, and the last term is the buoyancy. The inclusion of velocity gradients (the first term on the RHS) results in modifications to the virtual mass, the Stokes drag, and the Basset history terms to account for the effect of a nonuniform flow field. These velocity gradients correspond to the physical effect known as Faxen forces [27].

In certain engineering applications, where we are interested in global or macroscopic behavior of these suspensions, we model them as a single component fluid, usually represented by a single non-linear constitutive relation (for the stress tensor) where the material properties are functions of volume fraction of the particles. In these cases, we are not concerned about the amount of particles (whether dilute or dense) in the suspension and usually we are interested in the (total) flow rate, pressure drop, etc.; these can be obtained by solving the basic equations of motion. Also, there is only one constitutive relation which is needed for the stress tensor of the suspension. This approach, often called suspension rheology, in general cannot provide us with particle distributions, deposition, etc., unless certain convection-diffusion type equations are also used (see [28]).

From the statistical mechanics point of view, sometimes a particle dynamics approach (simulation) is used and sometimes a modified form of the kinetic theory of gases, as applied to rigid particles are used. These two techniques, especially with faster and more efficient computers have become more popular in the last few decade (see review articles dealing with the statistical theories by Herrmann [29, 30] and kinetic theories application to granular materials by Goldhirsh [31], or numerical simulation by Walton [32]).

In the next section, we will discuss and use the Stokesian Dynamics approach (a molecular dynamics-like method) and how it can be used to study the flow of a suspension.

2.2 Model Assumptions

We make several assumptions about the system of interest.

First, *the bubbles are assumed to be hard sphere particles*. Laboratory experiments show that the surfactants and stabilizers added to the base fluid maintain fairly spherical, stable, discrete bubbles in the flow regime typically encountered in the well [33]. The surfactants also cause the bubbles to

typically have minimal direct contact. It should be noted that treating bubbles as deformable elastic objects is an area of active research, e.g., [34], and infeasible for the large systems required here.

Second, *the suspending fluid (cement slurry) is considered Newtonian*. It is generally accepted that cement slurry has a yield stress and can behave in highly nonlinear manner [35, 36]. However, we emphasize that there exists no feasible way to simulate large collections of particles in non-Newtonian fluids while accounting for all particle positions. Therefore, while our simulations provide useful insights into some of the properties of the bubbles that control the real system behavior, particularly the clustering and structuring of bubbles, it is important to note that one should expect qualitative and quantitative differences compared to experiments.

Third, *the buoyancy of the bubbles is neglected*. Unlike aqueous foam solutions where the bubbles tend to rise due to buoyancy, bubbles in cement tend to remain in place unless they reach a critical size. This has been observed experimentally [37, 38]: in laboratory and field applications, the bubble sizes are kept below this critical size and were observed to remain where placed during curing [37]. This is reasonable considering that cement is a yield-stress fluid, and the yield stress must be overcome for the cement to flow around a bubble. In addition, the cement slurry particles, which act as surface active foaming materials, help keep the bubbles entrained [39].

2.3 Stokesian Dynamics

In a suspension of particles, the motion of each particle is transmitted through the suspending fluid. In the quasi-static (creeping flow) limit, this is felt immediately throughout the entire system by all the other particles. Therefore long-range effects should be carefully considered. For a dilute suspension of particles where the particles are far apart, the detailed shape and structure of the particles does not matter to leading-order. The velocity disturbance of one particle decays like a point force as $1/r^2$, where r is the radial distance from the particle [7]. When the particles are close together, the interaction of each particle pair is dominated by a pairwise force which comes from lubrication theory [40]. This force is on the order of $1/h$ for rigid particles with no-slip surfaces, where h is the gap between the particle surfaces. As the gap between the particles gets smaller, the force between them increases rapidly and the approaching particles cannot contact in finite time. In the setting of interest, both the far-field and the near-field interactions must be considered in hydrodynamic interactions. The Stokesian Dynamics method account for the far-field interaction through multipole expansions and for the near-field interactions through pairwise interactions [7]. This was later made more computationally efficient through the use of lubrication theory for the near-field interactions [41]. The FLD method further increased the efficiency by using fast approximate methods for the far-field interaction [8, 9]. The broader idea of developing multiscale methods for long-range interactions by decomposing into far- and near- field and then using multipole expansions for the far-field has been studied theoretically and numerically in the context of bubbly fluids [42] and electromagnetic interactions [43–45].

In a Newtonian fluid when the inertial term is neglected, we obtain the Stokes flow regime. The governing equation is a linear biharmonic equation, thereby allowing superposition. Given a flow with multiple particles, the flow due to each particle is given by a fundamental solution denoted by a Stokeslet, and the interaction between particles can be obtained by superposing appropriately

the Stokeslets solutions. This enables an *effective* pairwise interaction between particles where the influence of the mediating fluid is accounted through the Stokeslet. Bossis and Brady were the first to develop this idea and put this into the framework of pairwise molecular dynamics to enable the efficient simulation of suspensions [7, 46]. This method is denoted "Stokesian Dynamics".

For the Stokes flow regime, the viscous forces dominate and the inertial forces have negligible effects. The movement of a particle is governed by the equation [10, 46]:

$$\boldsymbol{m} \cdot \frac{\mathrm{d}\boldsymbol{U}}{\mathrm{d}t} = \boldsymbol{F}^H \tag{2.6}$$

Here, $\boldsymbol{U}$ is the generalized velocity vector of the particles with entries corresponding to both linear and angular velocities. The velocity vector therefore has 6 components, corresponding to linear and angular velocities along the Cartesian directions, for each particle. Correspondingly, $\boldsymbol{m}$ is the generalized moment of inertia matrix containing entries for mass as well as the rotational inertia and, $\boldsymbol{F}^H$ is the generalized force vector with entries for both force as well as moment. Contained in this hydrodynamic force vector are then the 6 Cartesian components of the force and torque for each particle.

Note that the hydrodynamic force $\boldsymbol{F}^H$ accounts for the flow-induced forces as well as forces due to other particles that are mediated through the fluid. Direct inter-particle forces, such as in charged systems or when they come directly in contact, and forces due to Brownian motion are not considered. In this study, there are no direct inter-particle forces, and Brownian forces are neglected because the particles are much bigger than the scale at which these are significant.

Consider a macroscopically uniform (i.e., affine) flow field $\boldsymbol{v}(\boldsymbol{x}) = \boldsymbol{A}\cdot\boldsymbol{x} + \boldsymbol{B}$, where $\boldsymbol{A}$ is the velocity gradient tensor and $\boldsymbol{B}$ is the mean velocity. The symmetric rate-of-strain tensor is defined $\boldsymbol{E}^\infty = \frac{1}{2}(\boldsymbol{A} + \boldsymbol{A}^T)$. The spin tensor is defined by $\boldsymbol{W} = \frac{1}{2}(\boldsymbol{A} - \boldsymbol{A}^T)$ and the axial vector corresponding to this skew-symmetric tensor is $\boldsymbol{w}$. The generalized far-field velocity $\boldsymbol{U}^\infty$ is defined by $\boldsymbol{B}$ and $\boldsymbol{w}$.

The hydrodynamic forces can be determined by the relationship between the particle velocities and forces due to the suspending fluid by:

$$\begin{pmatrix} \boldsymbol{F}^H \\ \boldsymbol{S}^H \end{pmatrix} = \mathcal{R} \cdot \begin{pmatrix} \boldsymbol{U}^\infty - \boldsymbol{U} \\ \boldsymbol{E}^\infty \end{pmatrix} \tag{2.7}$$

The symmetric first moment of the force, $\boldsymbol{S}^H$, is called the Stresslet. $\mathcal{R}$ is the resistance matrix, and contains the particle positions. The main outcome of Stokesian Dynamics and FLD is to more efficiently compute $\mathcal{R}$ so that large numbers of particles in a suspension can be simulated.

Both [46] and [7] compared two methods of adding particle interactions for a suspension: first, by constructing the mobility matrix $\mathcal{M}$ or by constructing the resistance matrix $\mathcal{R}$[1]. The computation time to construct $\mathcal{R}$ is significantly greater than for $\mathcal{M}$, but the particles overlap in using the mobility matrix, and the physics are not preserved. The reason for this issue with the $\mathcal{M}$ matrix is that it does not accurately capture the lubrication forces that prevent the particles from overlapping, and therefore $\mathcal{M}$ does not preserve the physics of the problem.

[1] $\mathcal{R}$ and $\mathcal{M}$ are not precisely inverses of each other but are closely related [40].

Brady and Bossis first construct the grand mobility matrix, $\mathcal{M}^{\infty}$, and invert it for an approximation to the resistance matrix to determine the far-field interactions. Inverting $\mathcal{M}^{\infty}$ approximates the far-field many-body interactions efficiently. However, $\mathcal{M}^{\infty}$ does not include the exact lubrication forces. To account for the exact near-field lubrication interactions, a resistance matrix can be used that has the exact two-body lubrication interactions, represented by $\mathcal{R}_{2B}$. However, this leads to double counting of some lubrication terms which must be subtracted; this is represented by the matrix $\mathcal{R}^{\infty}_{2B}$. This process can be represented by [7]:

$$\mathcal{R} = (\mathcal{M}^{\infty})^{-1} + \mathcal{R}_{2B} - \mathcal{R}^{\infty}_{2B} \tag{2.8}$$

Stokesian Dynamics preserves all the relevant physics of the problem but is computationally intense for systems with a large number of particles. To allow for larger systems while still maintaining the physics of the problem in accounting properly for far-field and near-field interactions, *Fast Lubrication Dynamics* (FLD) was developed [8, 9].

2.4 Fast Lubrication Dynamics (FLD)

The Fast Lubrication Dynamics [8,9] explicitly incorporates the lubrication interactions, following [41], but modifies the Stokesian Dynamics [7] to reduce the computation time. In FLD, the grand resistance matrix, denoted $\mathcal{R}_{FLD}$, is the sum of the near-field pairwise lubrication interactions and the far-field interactions from the diagonal components of an isotropic resistance tensor, $\mathcal{R}_{Iso}$. The lubrication terms come directly from [41].

The matrix $\mathcal{R}_{Iso}$ aims to approximate $(\mathcal{M}^{\infty})^{-1}$ in an efficient manner. To achieve this, $\mathcal{R}_{Iso}$ is assumed to have the form of a multiple of the identity matrix. The multiplicative factor – assumed to be a function of the volume fraction – is obtained by curve-fitting the short-time self-diffusivity results from FLD to those obtained from full Stokesian Dynamics. In this way, FLD aims to preserve the physics of the accurate Stokesian Dynamics approach while making the computation more efficient. The resistance matrix used in FLD is described by:

$$\mathcal{R}_{FLD} = \mathcal{R}_{Iso} + \mathcal{R}_{2B} - \mathcal{R}^{\infty}_{2B} \tag{2.9}$$

The full expressions of the lubrication force and torque were derived by [47], see also [40]. [41] derive expressions from the lubrication solutions to describe the modes of motion of both particles in the particle pair interaction.

We note below an important though subtle issue regarding the implementation of FLD in the molecular dynamics code LAMMPS (described further below). [41] give the expressions for the lubrication forces and torques of each particle in the pair interaction. Using these full expressions, including all the $\log$ terms, is important to accurately simulate monodisperse hard spherical particles with no-slip on their boundaries that are only interacting through hydrodynamic forces.

However, LAMMPS uses truncated expressions that leave out some terms. The truncated expressions in LAMMPS are generally used with other forces such as Brownian, colloidal, electrostatic, and so on. The error due to the missing terms can be negligible if other interactions dominate. However, we find that it is important to use the full expressions when computing the relative viscosity.

For instance, Figure 4 shows the relative viscosity as a function of volume fraction computed by Stokesian Dynamics [7, 46], FLD with truncated expressions [8], Ball and Melrose [41], and our FLD calculations. We notice, particularly as the volume fraction increases, that Stokesian Dynamics, our FLD calculations, and [41] all have good agreement. In contrast, the FLD calculations with the truncated expressions show increasingly significant deviations with the volume fraction.

2.5 Near-Field Lubrication Interactions for Particles of Different Sizes

Given a pair of particles 1 and 2, both with the radius a and a separation h between the particle surfaces, we can then write the lubrication forces $\boldsymbol{f}_i$ and torques $\boldsymbol{g}_i$ on each of the particles following [41]:

$$\boldsymbol{f}_1 = -\boldsymbol{f}_2 = -a_{sq}\mathbb{N}\cdot(\boldsymbol{v}_1-\boldsymbol{v}_2) - a_{sh}\left(\frac{2}{r}\right)^2\mathbb{P}\cdot(\boldsymbol{v}_1-\boldsymbol{v}_2) + \left(\frac{2}{r}\right)a_{sh}\boldsymbol{n}\times\mathbb{P}\cdot(\boldsymbol{\omega}_1+\boldsymbol{\omega}_2) \tag{2.10a}$$

$$\boldsymbol{g}_1 = -\left(\frac{2}{r}\right)a_{sh}\boldsymbol{n}\times\mathbb{P}\cdot(\boldsymbol{v}_1-\boldsymbol{v}_2) - a_{sh}\mathbb{P}\cdot(\boldsymbol{\omega}_1+\boldsymbol{\omega}_2) - a_{pu}\mathbb{P}\cdot(\boldsymbol{\omega}_1-\boldsymbol{\omega}_2) - a_{tw}\mathbb{N}\cdot(\boldsymbol{\omega}_1-\boldsymbol{\omega}_2) \tag{2.10b}$$

$$\boldsymbol{g}_2 = -\left(\frac{2}{r}\right)a_{sh}\boldsymbol{n}\times\mathbb{P}\cdot(\boldsymbol{v}_1-\boldsymbol{v}_2) - a_{sh}\mathbb{P}\cdot(\boldsymbol{\omega}_1+\boldsymbol{\omega}_2) + a_{pu}\mathbb{P}\cdot(\boldsymbol{\omega}_1-\boldsymbol{\omega}_2) + a_{tw}\mathbb{N}\cdot(\boldsymbol{\omega}_1-\boldsymbol{\omega}_2) \tag{2.10c}$$

$\boldsymbol{n}$ is the unit vector directed along the line connecting the center of particle 1 pointing toward particle 2, $\mathbb{N} := \boldsymbol{n}\otimes\boldsymbol{n}$, and $\mathbb{P} := \boldsymbol{I} - \mathbb{N}$. $\boldsymbol{v}$ and $\boldsymbol{\omega}$ are the velocity and the angular velocity, respectively, of the particles. The expressions in (2.10) provide the components of $\mathcal{R}_{2B}$. Noting that the left side – $\boldsymbol{f}, \boldsymbol{g}$ – in (2.10) corresponds to the generalized force $\boldsymbol{F}^H$, and is linearly related to $\boldsymbol{v}, \boldsymbol{\omega}$ that correspond to the generalized velocity $\boldsymbol{U}$.

Particle pairs have four modes of interaction that have been termed *squeeze* (sq), *shear* (sh), *pump* (pu), and *twist* (tw). These are shown schematically in Figure 1.

For two particles that have the same radius a, [41] derived the dominant pair interactions by first defining:

$$a_{sq} = 6\pi\mu a\left[\frac{1}{4h} + \frac{9}{40}\log\frac{1}{h} + \frac{3}{112}h\log\frac{1}{h}\right] \tag{2.11a}$$

$$a_{sh} = \pi\mu a^3\left[\frac{(2+h)^2}{4}\log\frac{1}{h}\right] \tag{2.11b}$$

$$a_{pu} = 8\pi\mu a^3\left[\frac{3}{160}\log\frac{1}{h} + \frac{63}{4000}h\log\frac{1}{h}\right] \tag{2.11c}$$

μ is the suspending fluid viscosity without the particles. The twist term from [41] was not included for our simulations as the contribution is negligible, i.e. $a_{tw} = 0$.

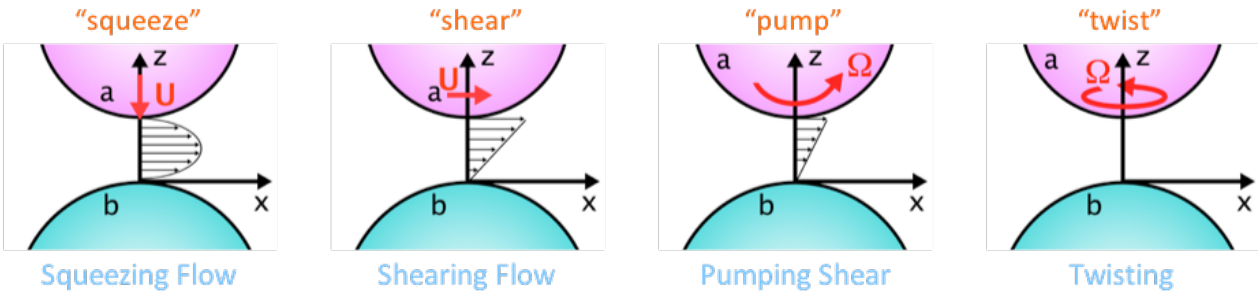

Figure 1: Particle pair interactions are shown for four motions of particle a relative to particle b.

For two particles with unequal radii a and b, the linear resistance depends on the ratio $\beta = \frac{b}{a}$. [40] give the equations for the force and torque on particle a, which is moving as shown in Figure 1, and particle b which is stationary. To determine the shearing terms, it is important to combine properly the shearing and shearing pump motion, following the description in [41]. To obtain the a_{sh} term, the force on particle a due to pure shearing motion must be multiplied by $\frac{(2+h)^2}{4}$ to include the Lorentz relationships as [41] have included in the Equations of 2.10. To obtain a_{pu}, g_{11} and g_{12} (from [47]) were combined (i.e. $g_{11} + g_{12}$) as done in [41].

The equations for a_{sq}, a_{sh}, a_{pu}, generated from the solutions shown in [40], and following [41] are now:

$$a_{sq} = 6\pi\mu a \left[\frac{\beta^2}{(1+\beta)^2} \frac{1}{h} + \frac{1+7\beta+\beta^2}{5(1+\beta)^3} \log\frac{1}{h} + \left(\frac{1+18\beta-29\beta^2+18\beta^3+\beta^4}{21\,(1+\beta)^4} \right) h \log\frac{1}{h} \right] \tag{2.12a}$$

$$a_{sh} = 6\pi\mu a^3 \left(1 + h + \frac{1}{4}h^2\right) \left[\frac{4\beta\,(2+\beta+2\beta^2)}{15\,(1+\beta)^3} \log\frac{1}{h} + \frac{4\,(16-45\beta+58\beta^2-45\beta^3+16\beta^4)}{375\,(1+\beta)^4} h \log\frac{1}{h} \right] \tag{2.12b}$$

$$a_{pu} = 8\pi\mu a^3 \left[\frac{4-\frac{1}{\beta^2}}{80\left(1+\frac{1}{\beta}\right)} \log\frac{1}{h} + \frac{132+24\frac{1}{\beta}-11\frac{1}{\beta^2}+24\frac{1}{\beta^3}-43\frac{1}{\beta^4}}{2000\left(1+\frac{1}{\beta}\right)^2} h \log\frac{1}{h} \right] \tag{2.12c}$$

We use these expressions in (2.10) to obtain $\mathcal{R}_{2B}$ for the case of two non-identical particles.

3 Numerical Simulations and Results

LAMMPS[2] – the Large-scale Atomic/Molecular Massively Parallel Simulator – is an open-source classical (non-quantum) molecular dynamics code developed and maintained at Sandia National Labs [48]. We use LAMMPS with the FLD method[3].

[2] lammps.sandia.gov

[3] As noted previously, we have extended LAMMPS to include the full expression for lubrication terms from (2.12).

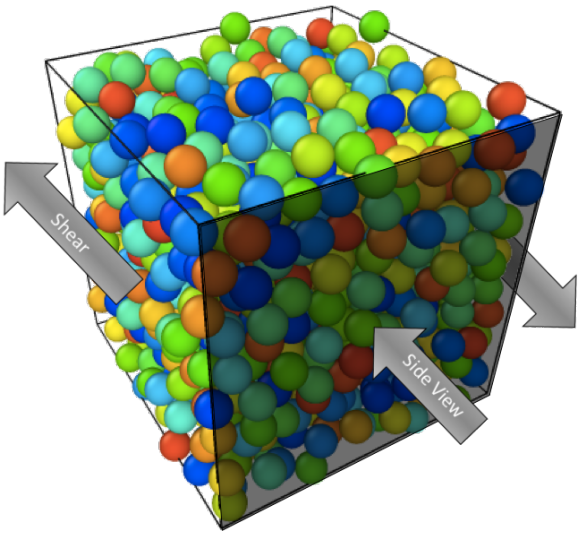

Figure 2: The particles are sheared in the direction shown and the images below are shown from the side view and looking through the whole sample.

3.1 Implementation of the Shearing Flow

Three dimensional simulations were performed using the Lees-Edwards periodic boundary conditions [49]. The velocity of each particle is a function of its position in the y-direction for strains imposed in the xy-direction. When a particle crosses the simulation boundary, the velocity is remapped to correspond to the new position in the simulation box[4]. The different suspensions were sheared as shown in Figure 2 until the stress had reached a constant value and a strain of 200 was reached. It was shown through testing different time steps, Δt (time units) that the dimensionless time step should be kept below 0.002 for the FLD simulations. An explicit time integration was used.

For the quasi-static setting, the only physical parameter is the total strain or the product of strain rate and timestep, $\dot{\gamma}$ (1/time units) $\times \Delta t$. For a given value of $\dot{\gamma} \times \Delta t$, the time-history of the stress and viscosity should be the same when time is appropriately re-scaled.

The stress in the system is calculated by summing the stresses computed for each particle. Ignoring the kinetic energy contributions that are negligible here, the stress on a particle is defined by [51, 52]:

$$\sigma_{i,\alpha\theta} = \frac{1}{V_i}[-\frac{1}{2}\sum_{n=1}^{N_p}(r_{1_\alpha}F_{1_\theta} + r_{2_\alpha}F_{2_\theta})] \tag{3.1}$$

Where α and θ run over the coordinate directions to compute the 6 components of the symmetric stress tensor. The sum runs over the N_p neighbors of the particle under consideration. $\boldsymbol{r}_1$ and $\boldsymbol{r}_2$ are the positions of every particle pair that has pairwise interactions, and $\boldsymbol{F}_1$ and $\boldsymbol{F}_2$ are the corresponding forces.

[4] See e.g. [50] for a discussion of this and [51] for the implementation.

For a simulation box with volume, V, the stress from each particle is summed to determine the total stress of the system of particles and is used to calculate the viscosity. With Lees-Edwards boundary conditions imposed, the relative viscosity, or more accurately, the viscosity ratio, is then calculated from the average total stress once the system has reached equilibrium:

$$\mu_{\text{relative}} = \frac{\mu_{\text{effective}}}{\mu} = \frac{\sum_i \sigma_{xy}}{\dot{\gamma}\mu V} \tag{3.2}$$

3.2 Generation of Initial Configurations of Particles

Particle systems were generated by randomly placing particles with a diameter of 1 in a $10\times10\times10$ box to create different volume fractions $(10\%, 20\%, 30\%, 40\%, 45\%, 50\%)$ of particles all having the same system volume. Once the particles are randomly placed, a soft potential is used with an energy minimization to remove overlaps in the initial configuration that are unphysical[5]. The energy of the soft potential is [51]:

$$E = A\left(1+\cos\left(\frac{\pi r}{r_{cut}}\right)\right), \quad r < r_{cut} \tag{3.3}$$

where r is the distance between particles, A is the pre-factor in energy units that was initially set low and ramped up, and r_{cut} is the cut off distance.

To avoid effects from the system size, testing was done to determine the appropriate system size that shows no further size dependence. The system sizes were progressively doubled in all coordinate directions until an appropriate size without size-dependence was achieved. It was determined that replicating the original system size four times in each direction eliminated system size effects. Once this configuration was replicated, the particles were then moved around using the random Brownian pair interaction in LAMMPS to make the particle arrangements random again. This step was not part of the dynamics but was simply to create a random placement of the particles after replicating the same arrangment of particles.

To create polydisperse particle systems, the monodisperse particle positions were used and the particle size was increased and decreased randomly on the monodisperse particles to add slight polydispersity to the particle sizes. Figure 3 shows the size distributions of the polydisperse particles. The system of polydisperse particles were then replicated and the positions randomized as described above.

3.3 Relative Viscosity/Viscosity Ratio

The relative viscosity or viscosity ratio was calculated with Equation (3.2). Simulations are run until an equilibrium is reached. The values of $\sum_i \sigma_{xy}$ are an average over the time period where the average stress is constant with time. The relative viscosity of monodisperse hard sphere particle suspensions as a function of volume fraction is shown in Figure 4. The values of [41], the more

[5]We emphasize that the soft potential is used only in generating a physical initial configuration, and plays no role once the simulation begins.

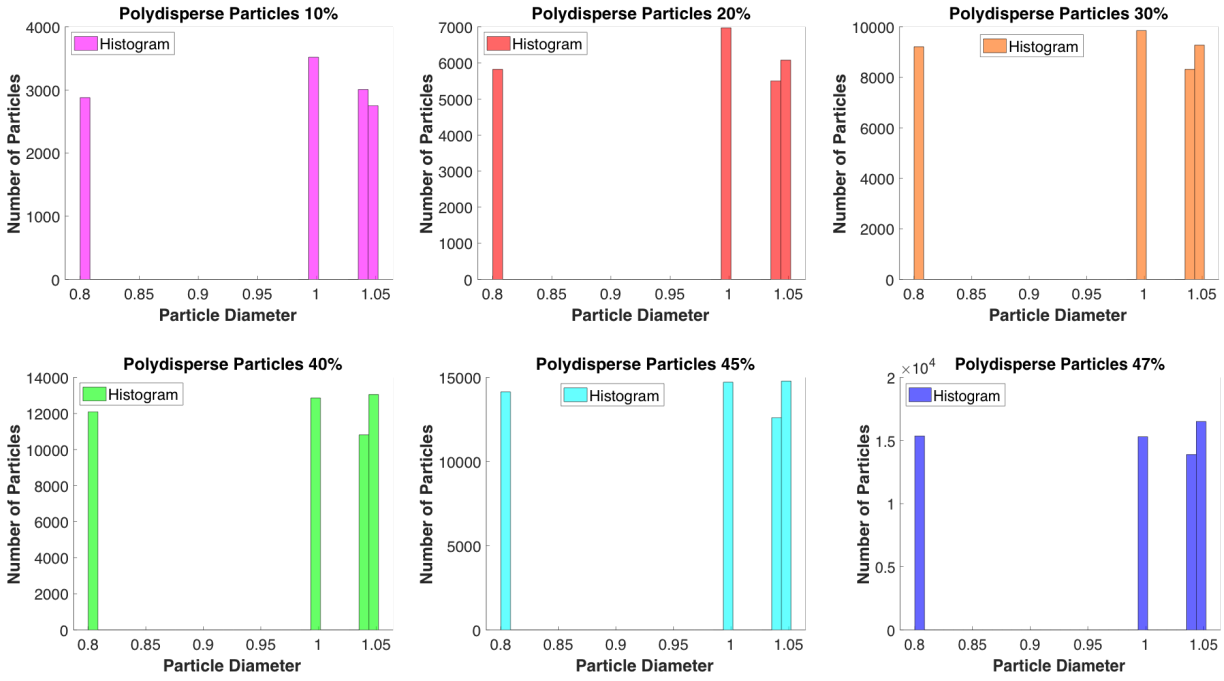

Figure 3: Particle size distribution of the slightly polydisperse particles.

accurate Stokesian Dynamics of [7, 46], and the FLD with truncated expressions of [8] are shown in black. Ball and Melrose simulated hard sphere suspensions using just the squeeze term so only volume fractions as low as 20% could be simulated. The squeezing force dominates in close-range interactions but Ball and Melrose were able to simulate hard sphere suspensions at 20% and higher and the results compare well to higher accuracy simulation methods, such as Stokesian Dynamics [7, 46]. To avoid particle overlaps, they utilize a smaller and smaller time step allowing particles to approach close to each other without overlap during the simulations, and so preserve the physics of the problem. Stokesian Dynamics should give the most accurate results but the computation time of Stokesian Dynamics limits the number of particles that can be used. To reduce computation time, the FLD method was then developed. The original FLD method implemented into the current distribution of LAMMPS includes truncated versions of Equations (2.11a), (2.11b), and (2.11c) to only include up to the first $\log$ term in each Equation. The truncated FLD pair interactions – that are the current implementation in LAMMPS (Original FLD) – resulted in higher values and match those reported in [8]. The relative viscosity calculated from simulations performed with the truncated resistance terms deviate from the results of Ball and Melrose and Stokesian Dynamics, especially at higher volume fractions. However, when we implemented the correct full expressions for the resistance terms into LAMMPS, the match between our results and Stokesian Dynamics was closer, even at the higher volume fractions.

Three different simulation box strain rates were tested to determine the influence of the shear rate. The same time step was used in all three cases. The same input configurations of particles was used for all three simulation sets. The simulations run with $\dot{\gamma} \times \Delta t$ values of 1×10^{-5} and 1×10^{-6} were all run until the strain reached 200 for all volume fractions shown. Due to time limitations on the computing resource, the simulation sets run with $\dot{\gamma} \times \Delta t$ of 1×10^{-7} were only strained to a

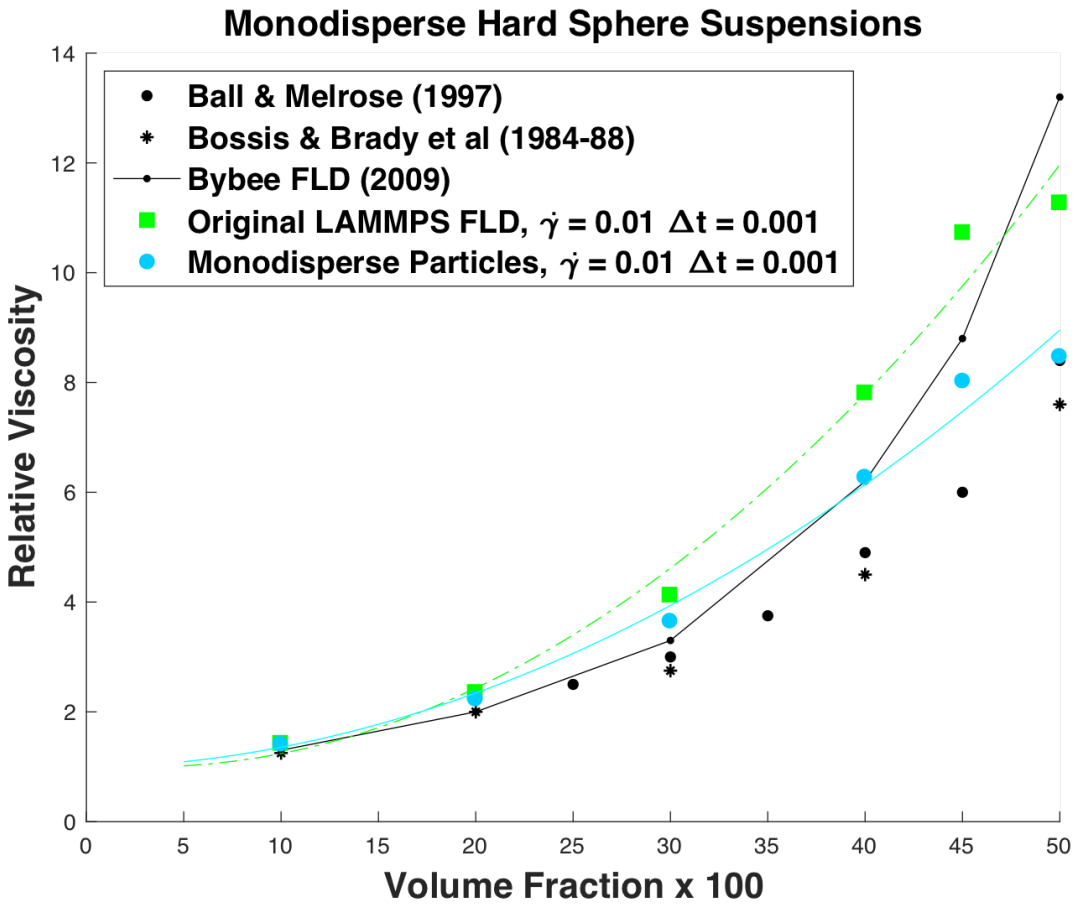

Figure 4: The results reported previously are shown in black. The results of the simulations reported here are shown in color. When we implemented the correct full expressions for the resistance terms into LAMMPS, the match between our results and those of Ball and Melrose (1997) and Brady and Bossis (1984) was closer, even at higher volume fractions, unlike Bybee (2009) and the original LAMMPS FLD implementation. The $-\cdot$ (Original FLD implementation in LAMMPS) and $-$ lines (Simulations with full correct expressions) are second order polynomial fits through the simulation data. Both simulation sets were run with the same initial particle data sets.

value of 20, which corresponds to the same length of simulation time as the $\dot{\gamma} \times \Delta t = 1 \times 10^{-6}$. However, the values of stress used to calculate the viscosity is an average of those values once the total stress have come to equilibrium, which occurs early on in the simulations. So even if the simulations were not strained the same amount, the viscosity should not be affected in an appreciable way. The results show that the variation of shear rates did not significantly impact the relative viscosity for the cases tested and shown in Figure 5. In these simulations, we assume that the particles maintain their spherical shape. Elongation of the particles due to shearing can influence the viscosity. Particle surface properties also can impact the effects of shearing on the viscosity. In cement slurry systems, for example, the rheology is dependent on shearing and resting history. When cements are at rest, particles within the suspension can flocculate together due to

random movements [35,36,53]. Shearing the suspension serves to break apart these particle clusters and is thought to lend to the shear thinning that occurs with time [35, 36, 53]. In the simulations shown herein, these properties are not included, which could be why the shear rates shown do not have an impact on the relative viscosity.

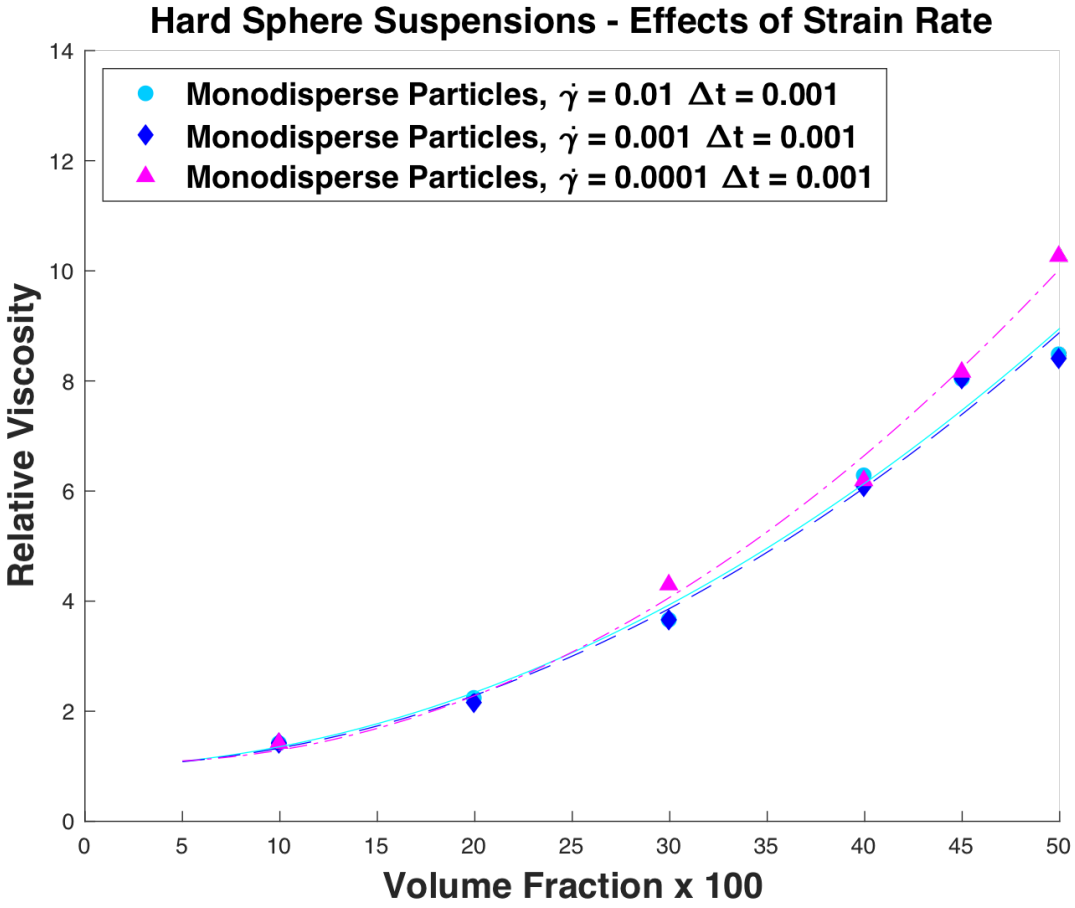

Figure 5: Results are shown for three different strain rates. The simulation sets were run with the same initial particle configurations.

Figure 6 compares the relative viscosity of the monodisperse particles to the slightly polydisperse particles. To create the particle inputs of the polydisperse particle sets, the monodisperse particle inputs were used but random particle sizes were decreased to a diameter of 0.802 and other particle sizes were randomly increased to a diameter of either 1.0495 or 1.0396, and the remaining particles kept a diameter of 1.0. The change in the particle sizes from the monodisperse particles with a diameter of 1.0, was a slight change to explore the effects that the particle size distribution has on the particle suspension properties. For the simulations explored here, the relative viscosity was not significantly impacted by the polydispersity added. The stress per particle that is used to calculate the relative viscosity is a function of the force between the particle pairs and the distance between their centers. The difference in the particle sizes is considered in calculating the force (Equations 2.12) but there is not a lot of disparity in the particle sizes. The center to center distances between

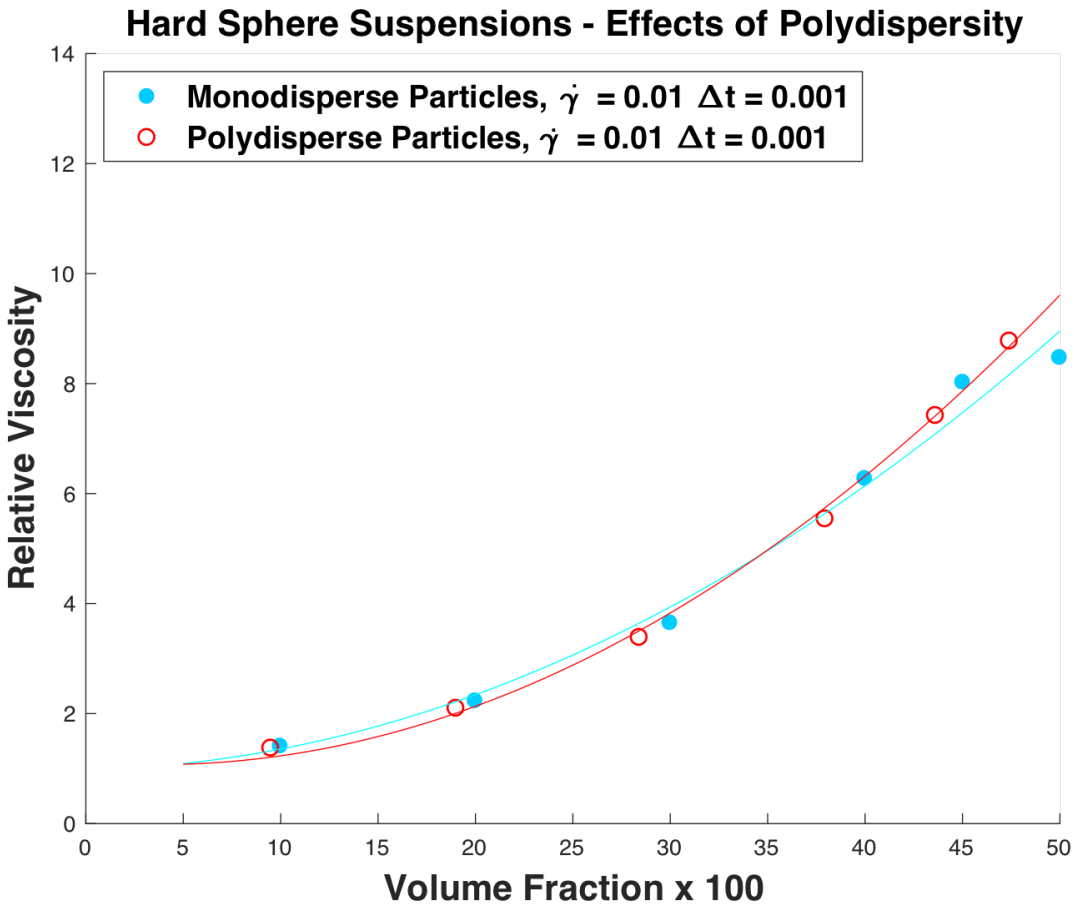

Figure 6: Results are shown for hard sphere suspensions of monodisperse (solid circles) and polydisperse (open circles) particles.

particles may also average out so that the same overall average stress that is calculated is not very different between the polydisperse and monodisperse particles.

3.4 Dependence of Structuring on Monodisperse vs. Polydisperse

To explore the effects of the particle volume fraction on particle rearrangement and structuring, the monodisperse particle placements from the 50% volume fraction, having a diameter of 1.0, was used to create lower volume fractions of particles by reducing the particle diameter of all particles. The volume fractions created correspond to 46%, 47%, and 48%, with diameters of 0.973, 0.980, and 0.99, respectively, to determine at what volume fraction the structuring is significant. Simulations of the monodisperse particles show structuring of the particles at a particle volume fraction of around 47% as shown in Figure 7. These results are consistent with [41]. A 48% volume fraction of particles had even more structuring. The relative levels of structuring between these volume fractions can be seen in Figure 7 and Figure 8. Figure 7 shows the final particle configurations at

the last timestep. All particles are shown in the figures and the perspective is a view from the side as indicated in Figure 2. The particles are shown at half their size so that the structures in the systems can be visualized. The colors of the particles show how many other particles are near by and are an indication of the particle structuring in a local region. The red particles show a higher coordination and level of structuring and the blue particles indicate no or little coordination with that particular particle's neighbors. In larger particle systems, the structuring may not be qualitatively or visually evident so the coordination number can be used to identify local regions of structuring. The coordination number is the sum of neighbors located within a distance of 1.5 from particle center. The coordination number for each particle was calculated using OVITO's[6] [54] computation of the coordination number and corresponding radial distribution function for each system of particles. Figure 8 shows the evolution of structuring over time. Three timesteps are shown in the figure for the initial and the final configurations and at the midpoint. The color corresponds to the level of coordination, where the red particles show a higher level of structuring and blue indicates less coordination. The radial distribution function is also shown for each time step and corresponds to the level of structuring of the whole system. The thinner, taller peak is indicative of more overall system structuring.

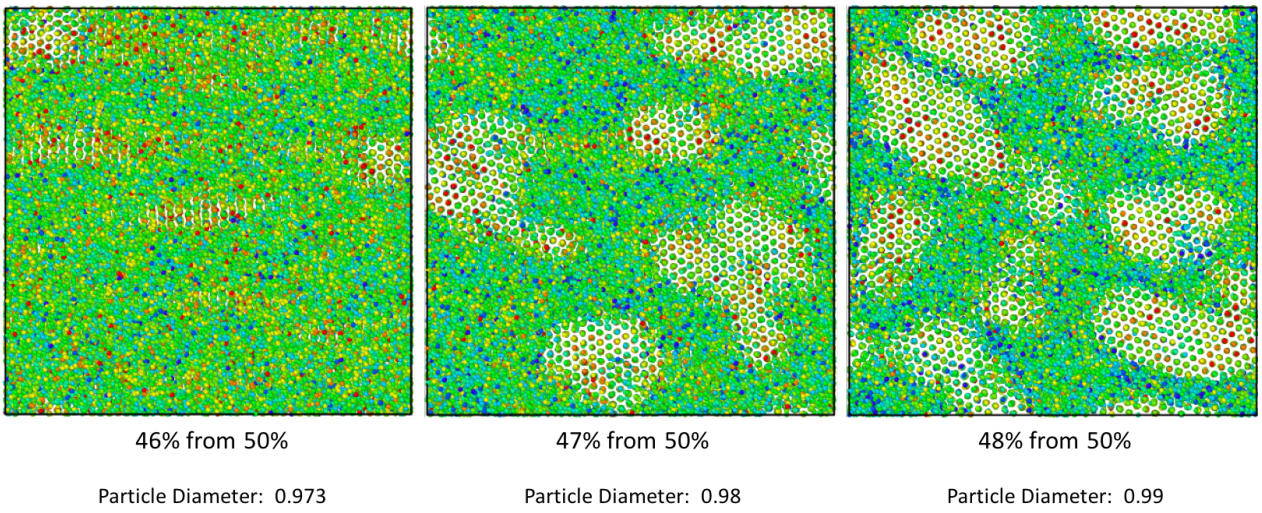

Figure 7: Comparison of structuring of monodisperse particles at three different volume fractions. The structuring is indicated by particles aligning along a single line and are seen as a single particle from the view point. The structuring increases with volume fraction. The particle configurations were made by reducing the monodisperse particle size from a 50% volume fraction of particles so that all particles are starting from the same configuration. The final configuration is shown. Particles are shown at half size.

By adding a small level of variation in the particle sizes to the same particle positions as the monodisperse particles, a comparison can be made between the monodisperse particles and the polydisperse. Because the monodisperse particles show structuring to begin and become noticeable at a volume fraction of 47%, a 47% volume fraction was used for comparison between the monodisperse and polydisperse particles. The polydisperse 47% by volume fraction of particles

[6] http://ovito.org/

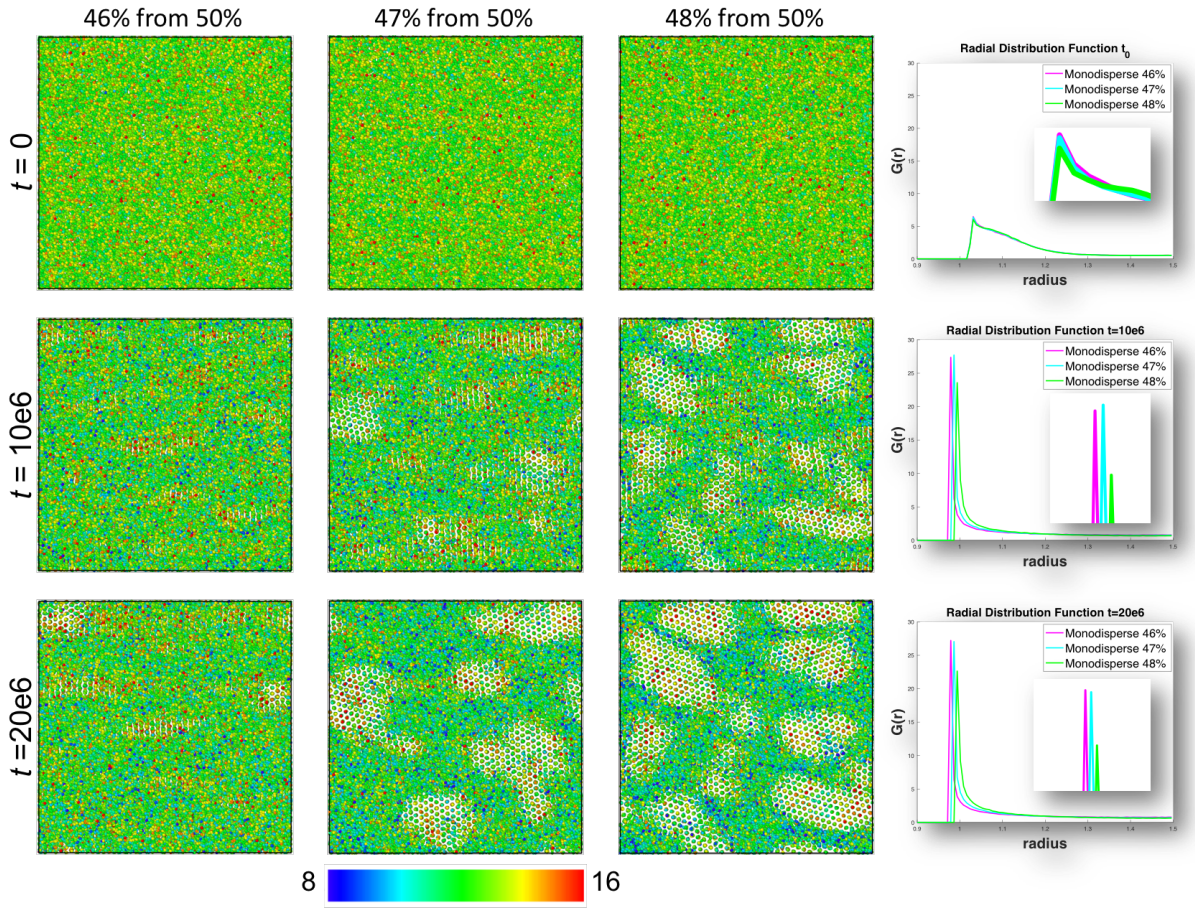

Figure 8: The Radial Distribution Function is shown at three different times, representing the initial configuration, the configuration at the mid-point and the configuration at the end of the simulation. The color corresponds to the particle coordination number. The side shown is the view indicated in figure 2.

system, did not show particle clustering or structuring after shearing. Figure 9 shows the three-dimensional simulation box and the particles at 47% by volume fraction of the monodisperse and polydisperse systems. The initial, random configuration of particles is shown with the final configuration at the end of the simulations. The direction of shear is indicated in the figure and particle alignment relative to the direction of shearing can be seen in the monodisperse system. The particles begin to align and form chains of particles. This can also be observed from the side view of the simulation box shown in Figure 10. From this perspective, the particles can be seen to align in a structured pattern similar to a crystal. One region of structuring is indicated with an ellipse. The particles are shown at half size in the inlaid image, where it is evident that the alignment extends throughout the length of the simulation box. In contrast, the polydisperse particles remain in a random configuration after shearing to the same strain value. In Figures 9 and 10 the color is only indicative of the particle size to emphasize the level of polydispersity relative to the monodisperse particles. As discussed in the previous section, the slight polydispersity did not have an appreciable effect on the relative viscosity, but there is a clear difference in the propensity to form structuring

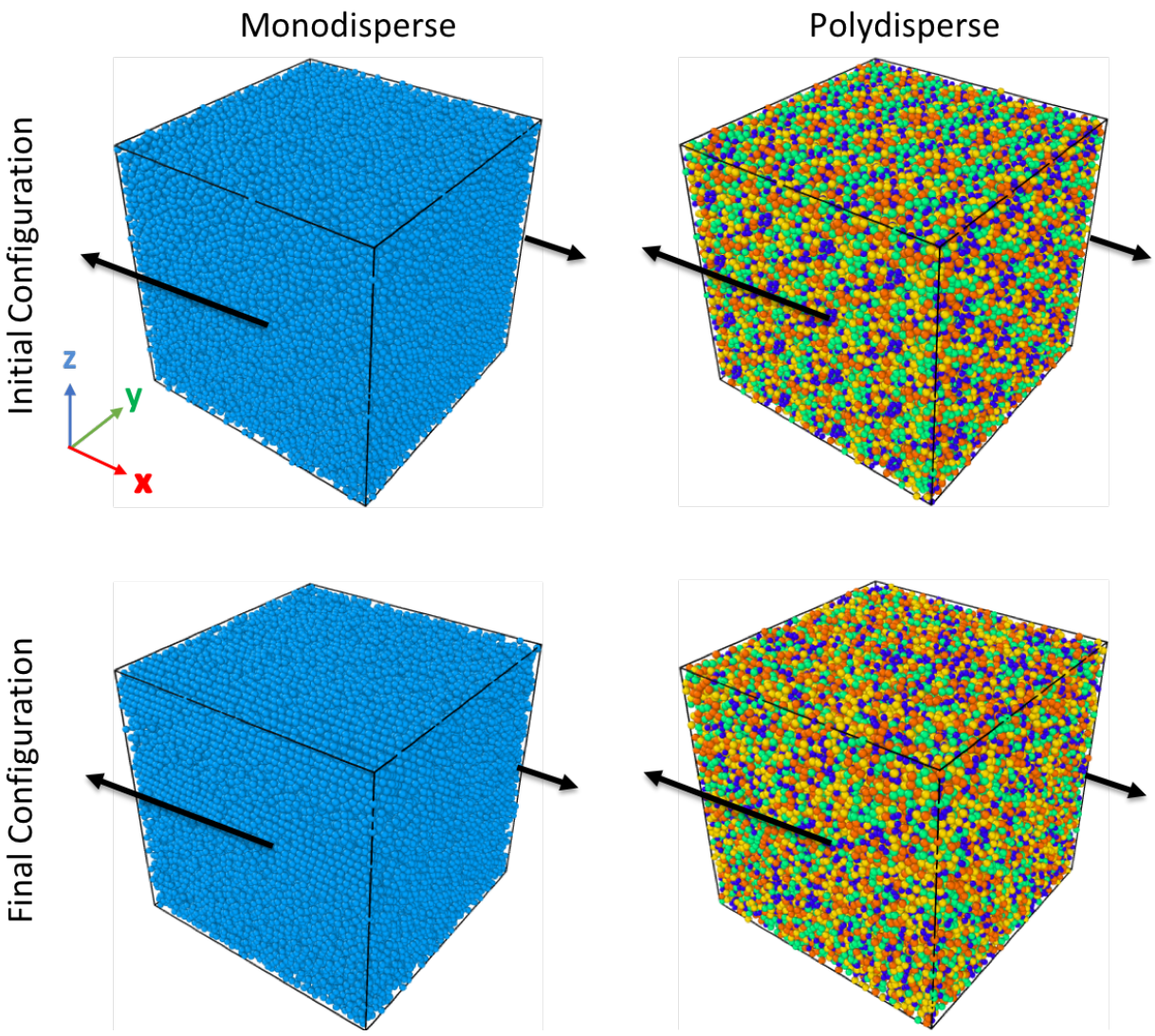

Figure 9: The initial and the final configurations of two 47% by volume fraction of particles systems. Monodisperse and polydisperse particle configurations are compared. The color corresponds to the particle size.

under imposed shearing between the monodisperse and polydisperse particles.

4 Discussion

A key finding of this paper is that even a small amount of polydispersity in the particle size distribution reduces structuring of the particles during a shearing Couette flow. Real systems, including foamed cements, have natural polydispersity. The goal is to keep particles dispersed after the flow has started and it seems that the polydispersity helps to maintain the dispersion. We also find that

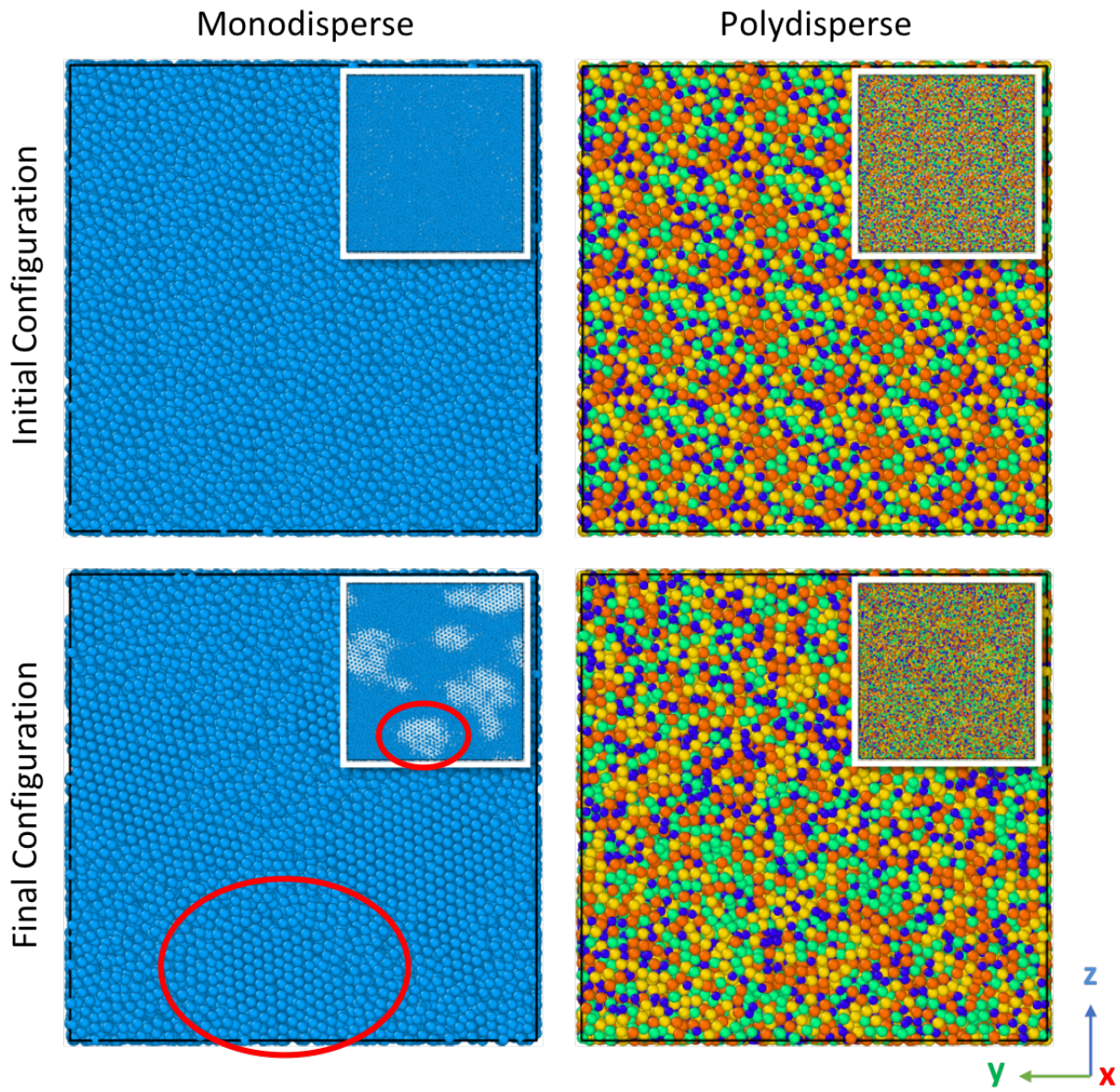

Figure 10: The initial and the final configurations of two 47% by volume fraction of particles systems. Monodisperse and polydisperse particle configurations are compared. The color corresponds to the particle size. The side shown is the view indicated in figure 2. The insert shows the particles at half size, where the structuring is more apparent. The circled region indicates one of the regions where structuring occurred in the particles. The particles form a line of particles in the x-direction.

the relative viscosity was minimally affected by adding the small amount of polydispersity. The effect of adding bubbles or particles to fluids is an increase in the viscosity, and therefore it is beneficial that the relative viscosity is not dependent on this level of polydispersity.

A key assumption that we have made here is that the fluid is Newtonian. This assumption is

essential for the Stokesian Dynamics method. In essence, the Newtonian assumption leads – in the Stokes' flow limit – to a linear problem. The linearity enables the use of superposition techniques – using fundamental solutions such as Stokeslets – that are specific to linear problems.

Cement slurry, on the other hand, is well known to behave as a non-Newtonian fluid [35,36]. However, there exists no method analogous to Stokesian Dynamics for the non-Newtonian setting since superposition cannot be used. Instead, one must solve, at a given time, the continuum mechanical balance of linear momentum[7] with a nonlinear constitutive response, $\boldsymbol{\sigma}(\boldsymbol{x},t) = \hat{\boldsymbol{\sigma}}(\phi, \boldsymbol{E})$, and with a large number of bubbles / particles embedded in the solution domain. Further, one must compute – at every time – the net force on all the bubbles / particles, and move them appropriately. Then the balance of momentum equation must be solved again, and so on. This is clearly a completely unfeasible problem.

A potential alternate approach for the future is to use homogenization methods, e.g. [55–59] that have also been used to similar ends. While these have the important advantage that non-Newtonian systems can tractably be solved numerically, they do not track individual bubbles / particles. Therefore, detailed insights into the structuring process cannot easily be resolved using these methods. An important goal for the future is to develop mixture theory-based models that include additional continuum scale fields (or internal variables) that track the structuring, possibly following ideas from [60].

We have focused our attention here on Couette flows using the Lees-Edwards method. Future work will look at a more general class of flows that generalize the Lees-Edwards method [50,61]. Like the Lees-Edwards method, this general class of flows are also exact solutions of particle dynamics.

Ongoing experimental efforts have the ability to study the bubble sizes and their typical distribution of sizes in the well, by producing foamed cement samples and then using Computed Tomography scanning to quantify bubble sizes, their size distribution, and their initial distribution within the sample relative to other bubbles [37,38]. Future work will continue to compare the particle dynamics simulations with experimental observations.

It would be very interesting to investigate higher volume fractions. However, it is difficult to create initial conditions of monodisperse particle systems of randomly placed particles above 50% volume fraction in the approach used here. The maximum packing fraction of ordered spheres is roughly $\sim 34\%$ to $\sim 74\%$ – depending on sphere packing pattern [62] – and these packings are uniform. A random arrangement of sphere packing when compressed has a maximum packing fraction of $\sim 64\%$ [63]. Therefore, an initial condition with not too much polydispersity that approaches these volume fractions, tends to become more ordered. Our current efforts involve the use of methods to create lognormal particle size distributions of randomly placed particles that do not overlap, but there are a number of unsolved challenges in achieving this.

[7] Here, $\boldsymbol{\sigma}$ is the stress field and $\boldsymbol{v}$ is the velocity field.

Acknowledgments

Kaushik Dayal acknowledges an appointment to the National Energy Technology Laboratory Faculty Research Participation Program sponsored by the U.S. Department of Energy and administered by the Oak Ridge Institute for Science and Education. We thank the National Science Foundation for support through the Extreme Science and Engineering Discovery Environment (XSEDE) resources. This work used the XSEDE Bridges Computing Resources provided at the Pittsburgh Supercomputing Center through TG-DMR160018. We thank the anonymous reviewer for a number of comments that improved the manuscript.

References

[1] N. Loeffler, "Foamed Cement: A Second Generation," in *Permian Basin Oil and Gas Recovery Conference*, 1984.

[2] J. de Rozieres and T. J. Griffin, "Chapter 14 Foamed Cements," in *Well Cementing* (E. B. Nelson, ed.), pp. 14.1 – 14.19, Schlumberger Educational Services, 300 Schlumberger Drive, Sugar Land, Texas 77478, 1990.

[3] American Petroleum Institute, "Isolating Potential Flow Zones During Well Construction - API Standard 65 Part 2," 2010.

[4] L. Tan, G. Ye, E. Schlangen, and K. Van Breugel, "Coupling of hydration and fracture models: Failure mechanisms in hydrating cement particle systems," *Particle and Continuum Aspects of Mesomechanics*, pp. 563–571, 2007.

[5] L. K. Tan, E. Schlangen, and G. Ye, "Simulation of failure in hydrating cement particles systems," vol. 348, pp. 737–740, 2007.

[6] NETL, "Tbd." Internal Research to be published, 2019.

[7] J. F. Brady and G. Bossis, "Stokesian dynamics," *Annual review of fluid mechanics*, vol. 20, no. 1, pp. 111–157, 1988.

[8] M. D. Bybee, *Hydrodynamic Simulations of Colloidal Gels: Microstructure, Dynamics, and Rheology*. PhD thesis, University of Illinois at Urbana-Champaign, 2009.

[9] A. Kumar, *Microscale Dynamics in Suspensions of Non-Spherical Particles*. PhD thesis, University of Illinois at Urbana-Champaign, 2010.

[10] A. Kumar and J. J. L. Higdon, "Origins of the anomalous stress behavior in charged colloidal suspensions under shear," *Physical Review E - Statistical, Nonlinear, and Soft Matter Physics*, vol. 82, no. September, pp. 1–7, 2010.

[11] S.-l. Soo, "Fluid dynamics of multiphase systems," *WALTHAM, MASS, BLAISDELL PUBLISHING CO, 1967. 524 P, 206 FIG, 8 TAB, 886 REF.*, 1967.

[12] G. B. Wallis, "One-dimensional two-phase flow," 1969.

[13] C. Truesdell, "Rational thermodynamics," 1984.

[14] R. Bowen, "Theory of mixtures," in *Continuum physics (Vol. III)* (A. Eringen, ed.), p. 1, New York: Waltham: Academic Press, 1976.

[15] R. Atkin and R. Craine, "Continuum theories of mixtures: basic theory and historical development," *The Quarterly Journal of Mechanics and Applied Mathematics*, vol. 29, no. 2, pp. 209–244, 1976.

[16] K. R. Rajagopal and L. Tao, *Mechanics of mixtures*, vol. 35. World scientific, 1995.

[17] M. Massoudi, "A note on the meaning of mixture viscosity using the classical continuum theories of mixtures," *International Journal of Engineering Science*, vol. 46, no. 7, pp. 677–689, 2008.

[18] M. Massoudi, "A mixture theory formulation for hydraulic or pneumatic transport of solid particles," *International Journal of Engineering Science*, vol. 48, no. 11, pp. 1440–1461, 2010.

[19] M. Massoudi, "On the importance of material frame-indifference and lift forces in multiphase flows," *Chemical Engineering Science*, vol. 57, no. 17, pp. 3687–3701, 2002.

[20] M. Massoudi, "Constitutive relations for the interaction force in multicomponent particulate flows," *International Journal of Non-Linear Mechanics*, vol. 38, no. 3, pp. 313–336, 2003.

[21] A. C. Eringen, *Nonlocal Continuum Field Theories*. Springer Science & Business Media, 2007.

[22] C. Crowe, M. Sommerfeld, Y. Tsuji, *et al.*, "Multiphase flows with," 1998.

[23] R. Clift, "Bubbles," *Drops and Particles*, 1978.

[24] S. Sadhal, P. Ayyaswamy, and J. Chung, "Transport phenomena with bubbles and drops," 1997.

[25] C. Tchen, "Mean value and correlation problems connected with the motion of small particles suspended in a turbulent fluid," 1947.

[26] M. R. Maxey and J. J. Riley, "Equation of motion for a small rigid sphere in a nonuniform flow," *The Physics of Fluids*, vol. 26, no. 4, pp. 883–889, 1983.

[27] J. Happel and H. Brenner, "Low reynolds number hydrodynamics, noordhoff int," *Publishing, Leyden, Netherland*, vol. 235, 1973.

[28] W.-T. Wu, N. Aubry, J. F. Antaki, M. L. McKoy, and M. Massoudi, "Heat transfer in a drilling fluid with geothermal applications," *Energies*, vol. 10, no. 9, p. 1349, 2017.

[29] H. Herrmann, "Statistical models for granular materials," *Physica A: Statistical Mechanics and its Applications*, vol. 263, no. 1-4, pp. 51–62, 1999.

[30] H. Herrmann and S. Luding, "Modeling granular media on the computer," *Continuum Mechanics and Thermodynamics*, vol. 10, no. 4, pp. 189–231, 1998.

[31] I. Goldhirsch, "Rapid granular flows," *Annual review of fluid mechanics*, vol. 35, no. 1, pp. 267–293, 2003.

[32] i. O. Walton and R. Braun, "Stress calculations for assemblies of inelastic speres in uniform shear," *Acta mechanica*, vol. 63, no. 1-4, pp. 73–86, 1986.

[33] L. E. U. D. o. E. N. E. T. L. Dalton, O. R. I. for Science, Education);, A. Brown, Sarah (US Department of Energy National Energy Technology Laboratory, A. Moore, Johnathan (US Department of Energy National Energy Technology Laboratory, D. U. D. o. E. N. E. T. L. Crandall, and A. Gill, Magdalena (US Department of Energy National Energy Technology Laboratory, "Evolution Using CT Scanning : Insights From Elevated-Pressure Generation," no. January, pp. 1–11, 2018.

[34] A. Rahimian, S. K. Veerapaneni, D. Zorin, and G. Biros, "Boundary integral method for the flow of vesicles with viscosity contrast in three dimensions," *Journal of Computational Physics*, vol. 298, pp. 766–786, 2015.

[35] N. Roussel, "Steady and transient flow behaviour of fresh cement pastes," *Cement and Concrete Research*, vol. 35, pp. 1656–1664, 2005.

[36] D. Guillot, "Rheology of Well Cement Slurries," *Developments in Petroleum Science*, vol. 28, no. C, pp. 4–1–4–37, 1990.

[37] B. Kutchko, D. Crandall, J. Moore, M. Gill, D. McIntyre, E. Rosenbaum, I. Haljasmaa, B. Strazisar, R. Spaulding, W. Harbert, G. Benge, E. Cunningham, D. W. Lawrence, G. DeBruijn, and C. Gardner, "Field-generated foamed cement: Initial collection, computed tomography, and analysis," tech. rep., U.S. Department of Energy, National Energy Technology Laboratory, 2015.

[38] B. Kutchko, D. Crandall, M. Gill, D. McIntyre, R. Spaulding, B. Strazisar, E. Rosenbaum, I. Haljasmaa, G. Benge, E. Cunningham, G. DeBruijn, and C. Gardner, "Computed Tomography and Statistical Analysis of Bubble Size Distributions in Atmospheric-Generated Foamed Cement," Tech. Rep. August, 2013.

[39] R. J. Pugh, "Foaming, foam films, antifoaming and defoaming," *Advances in Colloid and Interface Science*, vol. 64, no. 95, pp. 67–142, 1996.

[40] S. Kim and S. J. Karrila, *Microhydrodynamics: Principles and Selected Applications*. Mineola, NY: Dover Publications, Inc., 2nd ed., 2005.

[41] R. C. Ball and J. R. Melrose, "A simulation technique for many spheres in quasi-static motion under frame-invariant pair drag and Brownian forces," *Physica A: Statistical Mechanics and its Applications*, vol. 247, no. 1-4, pp. 444–472, 1997.

[42] A. Sangani and A. Acrivos, "The effective conductivity of a periodic array of spheres," *Proc. R. Soc. Lond. A*, vol. 386, no. 1791, pp. 263–275, 1983.

[43] R. D. James and S. Müller, "Internal variables and fine-scale oscillations in micromagnetics," *Continuum Mechanics and Thermodynamics*, vol. 6, no. 4, pp. 291–336, 1994.

[44] Y. Xiao, *The influence of oxygen vacancies on domain patterns in ferroelectric perovskites*. PhD thesis, California Institute of Technology, 2005.

[45] J. Marshall and K. Dayal, "Atomistic-to-continuum multiscale modeling with long-range electrostatic interactions in ionic solids," *Journal of the Mechanics and Physics of Solids*, vol. 62, pp. 137–162, 2014.

[46] G. Bossis and J. F. Brady, "Dynamic simulations of sheared suspensions. {I.} General method," *J. Chem. Phys.*, vol. 80, no. 10, pp. 5141–5154, 1984.

[47] D. J. Jeffrey and Y. Onishi, "Calculation of the resistance and mobility functions for two unequal rigid spheres in low-Reynolds-number flow," *Journal of Fluid Mechanics*, vol. 139, no. -1, p. 261, 1984.

[48] S. Plimpton, "Fast Parallel Algorithms for Short – Range Molecular Dynamics," *Journal of Computational Physics*, vol. 117, no. June 1994, pp. 1–19, 1995.

[49] A. Lees and S. Edwards, "The computer study of transport processes under extreme conditions," *Journal of Physics C: Solid State Physics*, vol. 5, no. 15, p. 1921, 1972.

[50] K. Dayal and R. D. James, "Nonequilibrium molecular dynamics for bulk materials and nanostructures," *Journal of the Mechanics and Physics of Solids*, vol. 58, no. 2, pp. 145–163, 2010.

[51] *LAMMPS Users Manual*. Sandia National Laboratories, 2003.

[52] E. B. Tadmor and R. E. Miller, *Modeling materials: continuum, atomistic and multiscale techniques*. Cambridge University Press, 2011.

[53] P. F. G. Banfill, "Rheology of Fresh Cement and Concrete," *Rheology Reviews 2006*, vol. 2006, pp. 61–130, 2006.

[54] A. Stukowski, "Visualization and analysis of atomistic simulation data with ovito–the open visualization tool," *Modelling and Simulation in Materials Science and Engineering*, vol. 18, no. 1, p. 015012, 2010.

[55] R. Lipton and M. Avellaneda, "Darcy's law for slow viscous flow past a stationary array of bubbles," *Proceedings of the Royal Society of Edinburgh Section A: Mathematics*, vol. 114, no. 1-2, pp. 71–79, 1990.

[56] R. Lipton and B. Vernescu, "Homogenisation of two-phase emulsions," *Proceedings of the Royal Society of Edinburgh Section A: Mathematics*, vol. 124, no. 6, pp. 1119–1134, 1994.

[57] T. Gao, H. H. Hu, and P. P. Castañeda, "Shape dynamics and rheology of soft elastic particles in a shear flow," *Physical review letters*, vol. 108, no. 5, p. 058302, 2012.

[58] T. Gao, H. H. Hu, and P. P. Castañeda, "Rheology of a suspension of elastic particles in a viscous shear flow," *Journal of Fluid Mechanics*, vol. 687, pp. 209–237, 2011.

[59] R. Avazmohammadi and P. P. Castañeda, "Macroscopic rheological behavior of suspensions of soft solid particles in yield stress fluids," *Journal of Non-Newtonian Fluid Mechanics*, vol. 234, pp. 139–161, 2016.

[60] J. Christoffersen, M. Mehrabadi, and S. Nemat-Nasser, "A micromechanical description of granular material behavior," *Journal of applied mechanics*, vol. 48, no. 2, pp. 339–344, 1981.

[61] K. Dayal and R. D. James, "Design of viscometers corresponding to a universal molecular simulation method," *Journal of Fluid Mechanics*, vol. 691, pp. 461–486, 2012.

[62] C. F. Gauß, "Besprechung des buchs von la seeber: Untersuchungen uber die eigenschaften der positiven ternaren quadratischen formen usw," *Gottingensche Gelehrte Anzeigen*, vol. 2, pp. 188–196, 1876.

[63] C. Song, P. Wang, and H. A. Makse, "A phase diagram for jammed matter," *Nature*, vol. 453, no. 7195, p. 629, 2008.